Site Characterization by Geophysical Methods in The Archaeological Zone of Teotihuacan, Mexico

R. E. Chávez*

Instituto de Geofísica, UNAM. Cd. Universitaria, Circuito Exterior, 04510 México

M. E. Cámara

Depto. de Física Aplicada, Escuela Técnica Superior de Ingenieros Industriales, UPM, José Gutiérrez Abascal 2, 28006 Madrid, Spain

A. Tejero

Facultad de Ingeniería, Div. de Ciencias de la Tierra, UNAM. Cd. Universitaria Circuito Facultades, 04510 México

L. Barba

Instituto de Investigaciones Antropológicas, UNAM. Cd. Universitaria, Circuito Exterior, 04510 México

L. Manzanilla

Instituto de Investigaciones Antropológicas, UNAM. Cd. Universitaria, Circuito Exterior, 04510 México

In the present investigation, a geophysical study was carried out in the eastern flank of the Pyramid of the Sun to define potential continuations in this direction of a tunnel discovered beneath the western main entrance of this building. This man-made structure is one of the many extraction tunnels hollowed by the ancient Teotihuacans to obtain construction materials to build their city. Total field and high-resolution vertical gradient magnetic surveys were carried out. The spectral analysis of the total magnetic field enabled us to estimate the thickness of the alluvial cover over the basaltic flow as 3·3 m. It was also found that the main contribution to the observed magnetic field comes from the pyroclastic flow that covers the area of study. The horizontal gradient filter was applied to the low-pass filtered magnetic field to enhance magnetic contacts and structural boundaries. Inferred magnetic trends were related to fracture patterns within the basalts and pyroclasts, and low gradients provided an evidence of voids or tunnels. The Euler deconvolution method was applied as an attempt to confirm the above results. Using a structural index S=0, we determined the boundaries of main magnetic contacts as well as the interface between the basaltic flow and Las Varillas tunnel. Euler depths were found to range between 3 to 6 m, which represent the mean thickness of the basaltic flow.

Two parallel ground probing radar (GPR) profiles were surveyed in the NW-SE direction. One passes on top of the known location of a tunnel (Las Varillas) and a second one 10 m to the north, approximately. The tunnel's roof is well outlined at depths between 3·5 and 4 m. On the other hand, little evidences of other buried tunnels or extensions of the known one were found. The second profile depicts a more complex morphology for the pyroclastic sheet. Anomalies related to basaltic flow or eruptive centres are clearly observed. Both profiles depicted the sedimentary base at 3 m, on average. A resistivity profile was undertaken along the first GPR profile. A resistivity image was obtained, that showed the vertical and lateral distribution of the true resistivity. High resistivity values were associated with the tunnel location (Las Varillas). Its geometry could also be inferred, its top is found at about 4 m and extends 20 m in the profile direction to the west. Unfortunately, the depth to its base could not be estimated, since profile length was too short. The sediment-pyroclastic flow interface could also be delimited at a depth of 3 m.

*exprene@tonatiuh.igeofcu.unam.mx

Finally, a vertical magnetic field profile taken along the same surveyed line (GPR and resistivity) was inverted applying a two-dimensional algorithm. The initial model was estimated from GPR and resistivity interpretations. A simple model of Las Varillas tunnel was computed, which reasonably well satisfied geological and geophysical considerations.
© 2001 Academic Press

Introduction

Archaeological studies done in different regions of Prehispanic America, and in particular in central and southern Mexico have shown the importance conferred to the underground spaces by the different cultures that lived in the area. It is known that caves and tunnels have had a functional and religious meaning for ancient cultures. These features have been used as shelters, astronomic observatories, quarries, and sites for religious ceremonies, among others (Manzanilla *et al.*, 1994, 1996).

In particular, in the ancient city of Teotihuacan, the existence of a tunnel beneath the Pyramid of the Sun is well known (Heyden, 1975). This apparent man-made feature was built around 50 AD as an extraction tunnel, afterwards employed for ritual ceremonies. It is 100 m long starting at the western side of the Pyramid's base, 6 m beneath the surface and ends in a four-room chamber, almost beneath the building's apex. Archaeologists believed that this tunnel could extend further east, as earlier geophysical and geological studies suggested (Manzanilla *et al.*, 1994).

Basante (1982) described several tunnels found in the Valley of Teotihuacan. Soruco (1985) reported the existence of an astronomical observatory built inside a tunnel, behind the Pyramid of the Sun. Heyden (1981) commented the existence of other tunnels beneath distinct ceremonial centres in Teotihuacan, and their religious meaning. Archaeologists suppose that the Teotihuacans probably took the situation of tunnels into account in selecting the initial construction place of this ancient city (northeastern sector).

Geophysical methods are now currently employed to explore shallow structures to study hydrological basins (Campos-Enriquez, Flores-Marquez & Chávez, 1997), and cave detection on modern urban sites (Chávez, Tejero & Urbieta, 1998), among other applications on environmental geophysics. Similar approaches can be applied for archaeological investigations. A geophysical study was previously carried out towards the western (on top of the known tunnel) and the eastern flanks of the Pyramid of the Sun (Manzanilla *et al.*, 1994; Chávez *et al.*, 1994). Such a study led to partially explore and discover archaeological artifacts and human bones in Las Varillas tunnel (Manzanilla, Lopez & Freter, 1996), east of the pyramid. In order to characterize selected magnetic signatures, Chávez *et al.*, (1994) interpreted several magnetic anomalies towards the eastern flank of the Pyramid of the Sun.

Some were associated with basaltic pillars, generally surrounded by non-magnetic sediments. This confirmed the idea suggested by Barba (1995), that the Teotihuacans extracted the soft materials around the emission cones, until the hard basalt was reached.

In this study, the geophysical and geological work carried out during the last two years is reported. In this last phase of research a comparison between different geophysical prospecting methods is made. In particular, a more quantitative analysis of the geophysical data is achieved by applying different computational processes to enhance geological features masked in the data. Also, despite the geological complexity of the region, possible archaeological targets could be inferred, as well as evidences of tunnels that might have been used by the Teotihuacans.

Geological Setting

Milan (1990) assigned to the Middle and Late Miocene the age of the oldest rocks found in the Valley of Teotihuacan. Such rocks crop out at the Malinalco Volcano and are constituted by andesites. Extrusive rocks at the Patlachique Mountain correspond to the Early Pliocene. The rock composition varies from andesites to dacites, including pyroclastic flows and non-consolidated sequences conformed by lithic tuffs and pumice covered by lava flows. Figure 1 gives a schematic location of the pyroclastic flow in the vicinity of the City of Teotihuacan.

Pyroclastic and fluvial activity during the Pliocene developed non-differentiated deposits of clay and gravel. These are found at the top of the last horizons of lava flows, and are also interbedded with lavas and pyroclasts from the Quaternary. The yellowish tuffs outcropping in the surroundings of the archaeological site are part of such deposits. The Quaternary rocks in the Valley of Teotihuacan are represented by mafic volcanic rocks from eruptive events of the Cerro Gordo Volcano, located to the north of the ancient city. This geological structure is a strato-volcano composed of layers of lavas and stratified Plio-Quaternary volcanic ashes.

Part of the archaeological city of Teotihuacan stands on top of a uniform sequence of volcanic tuffs and conglomerates (Figure 1), where volcanic bombs are abundant in different shapes and sizes (0·2 to 2·5 m), mixed with fragments of basaltic rocks and debris. The Pyramid of the Moon and the Pyramid of the Sun are
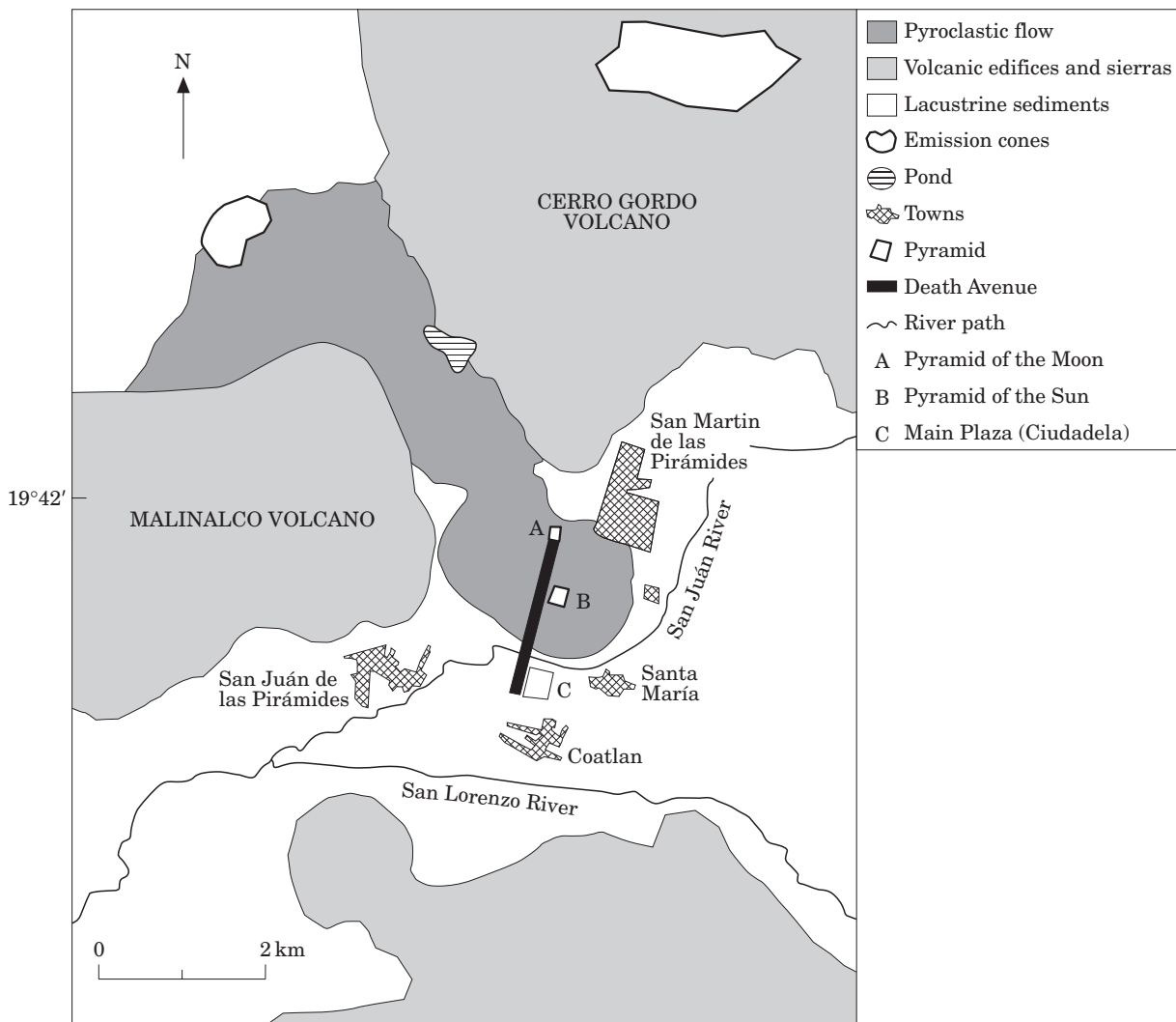
Figure 1. Geological overview of the archaeological site of Teotihuacan, Mexico. Location of main Pyramids (A) Sun and (B) Moon, and main plaza (C) the Ciudadela are shown. The tongue-shaped pyroclastic flow is displayed, Most of the ancient city was built on top it.

built on top of the pyroclastic flow to the north, while the Ciudadela (Central Plaza) was constructed over lacustrine sedimentary rocks to the south (Figure 1).

Alluvial, fluvial and lacustrine deposits are found in the central part of the valley, as well as in the small and main river paths (Figure 1 shows only two river paths, the San Juan and San Lorenzo rivers), whose sediments are found in eroded terraces. The sediments are conformed by grabbles, sands, and moods of alluvial origin conforming the valley (Milán, 1990). Mooser (1968) indicated the existence of tectonic faults delimiting the valley in the four directions. Magma scarps were produced along these faults during the volcanic activity, observed in the ranges around the valley. Cinder cones belong to the Quaternary age, according to Mooser. Such structures may be covered by subsequent lava flows. The analysis of aerial photographs reported a lobular flow within different topographic levels, which trends from north to south

between the Malinalco and Cerro Gordo volcanoes (Figure 1). This lava flow suddenly stops at the San Juan Teotihuacan River, at the end of The Street of the Dead (see Figure 1). Based in this evidence, Barba et al. (1990) suggested that the basaltic flow met water bodies in the central portion of the valley. Then, steam explosions could produce tunnels and cavities. Therefore, volcanic bombs abundant in the interior of tunnels and caves within the Valley of Teotihuacan should show evidence of strong dragging on their surface. However, bombs samples found in the interior of tunnels were examined, finding them almost intact, with no evidence of dragging on their surface.

On the other hand, Barba et al. (1990) mapped and described the presence of a series of depressions found to the northwest and to the east of the archaeological site, where entrances to tunnels were discovered. Such depressions follow apparent NW–E alignments that conspicuously divide the ancient city in two
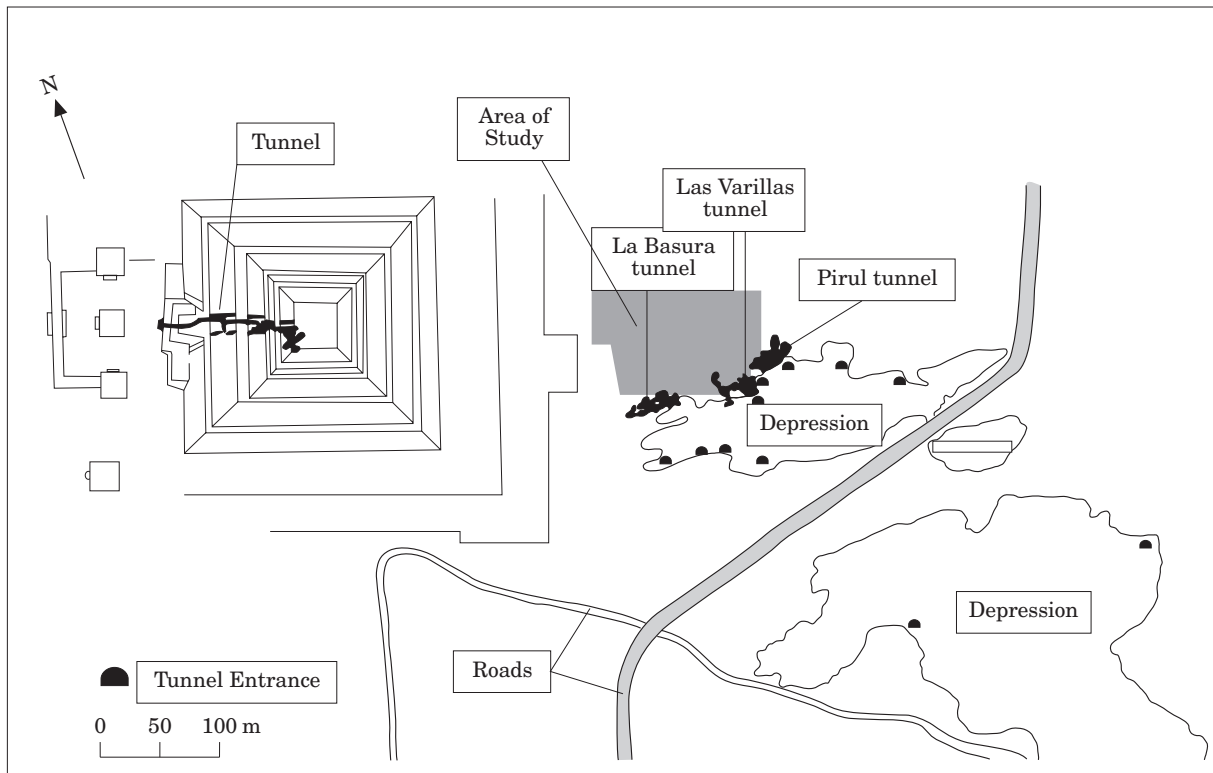
Figure 2. Location of area of study (square). Pyramid of the Sun is located to the west and depression with discovered caves to the east close to the area of study is shown. Observe the location of tunnel reported by Heyden (1975) beneath the Pyramid of the Sun.

portions. A few of these tunnel systems have already been studied in some detail, like the depression at Oztoyahualco (Arzate *et al.*, 1990), to the west of the ancient city. Barba (1995) found that the depressions are associated with fractures or extrusive centres, where magma flew. Also, cinder cones and emission centres were detected within the tunnels, astonishingly basaltic pillars supporting the tunnels' roof were found exposed, with no sign of volcanic tuffs and debris surrounding the pillar (Chávez *et al.*, 1994; Manzanilla, Lopez & Freter, 1996).

Therefore, Barba (1995) proposed that soft materials (pumice and tuffs) were extracted out from the tunnels, suggesting that these features were man-made. He compared the amount of material needed for building the city of Teotihuacan, and the soft components missing in the caves and tunnels surrounding the archaeological site. Results matched extremely well. Naturally, hard material like basalts and andesites were difficult for the ancient Teotihuacans to quarry with simple extracting tools. They were able to use only fragments of these igneous rocks. Such a remarkable discovery explains the location and the state of preservation of the volcanic bombs within the explored caves.

Geophysical Survey and Interpretation

The geological complexity of Teotihuacan led us to apply different geophysical methods to investigate possible extensions of caves and tunnels already known, and to further characterize the subsurface in the area of study. Measurements of total field magnetic observations as well as of its vertical gradient were carried out in the area of study. The first data set is useful to understand the magnetic properties of the subsurface rocks. The second one helps to enhance the position and boundaries of the causative magnetic bodies. GPR profiles were also employed to confirm the presence of cavities, tunnels and geological features, like basaltic pillars, faults, and so on. Finally, resistivity imaging (electric tomography) was applied to estimate the lateral and vertical distribution of resistivity.

Magnetic survey

A magnetic survey was carried out to the east of the Pyramid of the Sun (Chávez *et al.*, 1994). This survey covered an area of 160 m × 80 m, near a depression where some caves and tunnels have been explored recently (Figure 2). The equipment employed is a cesium magnetometer with a resolution of 0·1 nT. The sensor was set at 1·2 m height. A base proton magnetometer Geometrics G-816 was used to control the diurnal variation. Magnetic stations were taken at a 2 m interval, with observation lines (E–W oriented) separated by 2 m and 4 m. The survey comprised a total of 1386 magnetic observations.
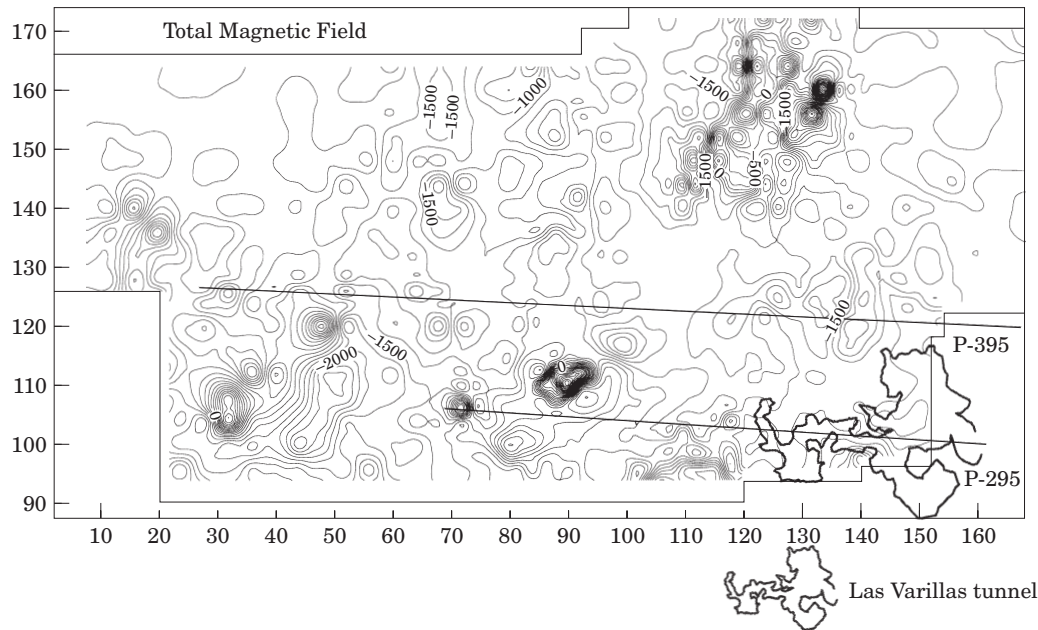
Figure 3. Residual magnetic field. High magnetic values depict the location of basaltic pillars (bottom) and emission cones (top-right). Location of GPR profiles P-295 and P-395 is shown. Las Varillas tunnel is projected to the surface (bottom-right). Contour interval is 250 nT.

We have subtracted the IGRF value (44,300 nT) for the year 1995·0 to the measured total magnetic field. The resultant residual field magnetic anomaly is displayed in Figure 3. High intensity anomalies are associated with eruptive centres of lava flows, which present NE–SW alignments. Areas displaying poor magnetization correspond to tuffs, volcanic ashes and pumice and soils. Drill-holes done in the area (Barba, 1995) reported a stratigraphic column that confirms this interpretation. Las Varillas tunnel has been projected to the surface and superimposed on the total field magnetic map (Figure 3). The tunnel's main entrance is found to the lower right, which also is the limit with the depression outlined in Figure 2. Depression walls are about 3 to 4 m in height at this point. The main access is 2 m in diameter, approximately. Low magnetic values may be associated with empty portions of that feature. However, the strong magnetic signal that corresponds to the basaltic pillars masks the low amplitude magnetic values from the tunnel.

The spectral analysis method has been applied to the magnetic data to estimate the mean depth to the magnetic sources (Spector & Grant, 1970). The power spectrum as a function of the radial wavenumber is shown in Figure 4. Spector & Grant (1970) demonstrated that the mean depth can be easily obtained by the following expression (Chávez, Flores-Marquez & Chávez, 1995):

$$\ln(\langle E(\mathbf{k})\rangle) = -2\pi H \mathbf{k}, \qquad (1)$$

where $\langle E(\mathbf{k})\rangle$ is the power spectrum, $\mathbf{k}$ is the radial wavenumber, and H is the mean depth. It is possible
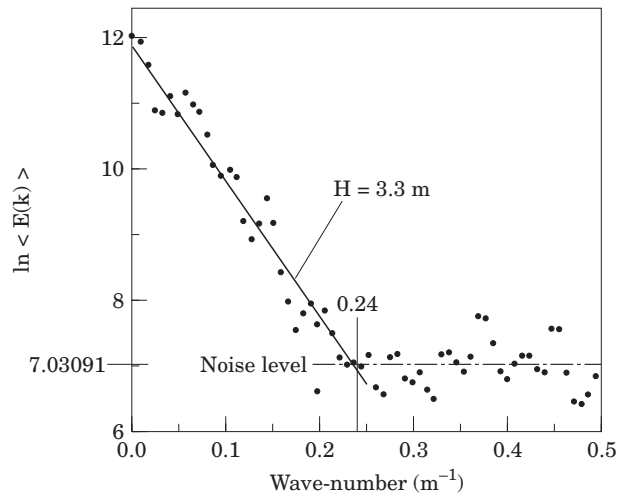
Figure 4. Spectral analysis plot. The spectrum of data (E(k)) from Figure 2 is plotted as a function of the radial wave number k. Observe that there is one main component in the magnetic field before k=0·24 m^{-1} (cutoff wavenumber). The reminder spectrum represents white noise due to interpolation and observational errors. Estimated depth for magnetic sources is 3·3 m, which is the depth to the top of the pyroclastic flow in the area of study.

to observe that the main contribution in terms of the wavenumber content in the magnetic signal of the observed field comes from the magnetized pyroclastic flow and basalts, which cover the area of study. Then, the slope given as m=2πH will give the depth estimate. A linear regression method is applied to calculate m, and the mean depth of 3·3 m for the magnetic sources is computed. This result can be associated with the
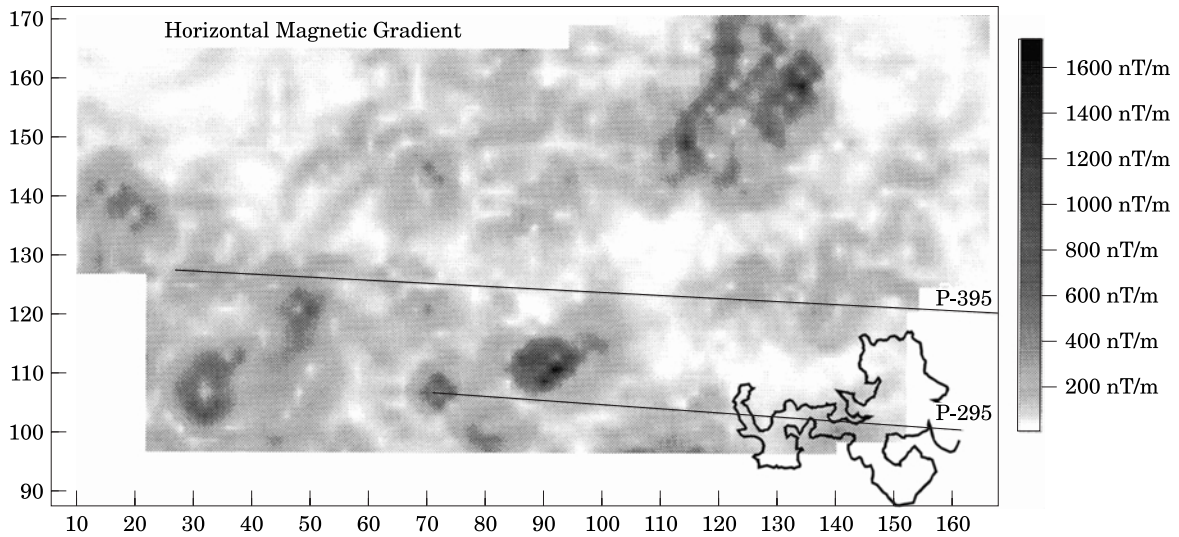
Figure 5. Horizontal gradient field. Main structural trends are nicely enhanced, in particular a semi-circular pattern can be seen to the northwest, and other lineaments in the NW–SE direction, probably related to fractures. In dark, location of emission cones and basaltic pillars are clearly seen. Low- and non-magnetic materials are shown in white.

depth to the sediment-pyroclast flow (or magnetic basement) interface. We can expect that beneath such depth tunnels can be found.

A filtering process was applied to the total field magnetic anomaly to amplify geometrical characteristics of the magnetic sources. The horizontal gradient operator is a function that enhances the horizontal extent of magnetic and gravitating bodies (Hildebrand *et al.*, 1995). The total field magnetic anomaly $T(x,y,z)$ can be expressed in terms of its horizontal T_x and T_y components as:

$$T_x(x,y,z) = \frac{\partial}{\partial x} T(x,y,z)$$

$$\qquad\qquad(2)$$

$$T_y(x,y,z) = \frac{\partial}{\partial y} T(x,y,z)$$

This operation can be simplified in the wavenumber domain, applying the Fourier transform to the total field anomaly $T(x,y,z)$ in terms of the wavenumbers p and q. The horizontal gradient operator is defined as:

$$T_p = -ipT(p,q)$$

$$T_q = -iqT(p,q) \qquad\qquad(3)$$

in terms of the p and q components of the Fourier transformed magnetic field $T(p,q)$. The vectorial sum of equation 3 will give the magnitude of the horizontal gradient field in Figure 5.

This map shows the boundaries of the emission centres (eroded emission cones as reported by Barba (1995)), located to the northern right hand-side of map, which are clearly defined in dark tones. Also, the emission centres and basaltic pillars to the south and

southwest can be observed. Low magnetic values depict a semicircular alignment, suggesting a fracture in the pyroclastic flow. Grey-to-white regions depict low-magnetic rocks, like tuffs, pumice and debris, which mostly surround basaltic pillars or other geological structures, and that the Teotihuacans extracted and employed as construction material. Voids and tunnels may be located within this soft material. The main chamber of Las Varillas tunnel is partially located within such an alignment, observed as a low magnetic gradient; the rest of the tunnel's bulk is not well resolved (Figure 5). This is due to the dimensions of minor chambers, which are small compared to the main one and to the magnetic resolution.

In order to estimate depths to magnetic sources, the Euler deconvolution technique is applied to the total field magnetic data. It is important to point out that this transformation is independent of the geographic position of the observed data. Therefore, reduction-to-the-pole is not needed. The Euler magnetic deconvolution (Reid *et al.*, 1990) can be written as:

$$(x-x_0)\frac{\partial T}{\partial x} + (y-y_0)\frac{\partial T}{\partial y} + (z-z_0)\frac{\partial T}{\partial z} = S(T-B), \quad (4)$$

where S is a structural index depending on the source geometry, and **B** is a background field. The coordinates (x_0, y_0, z_0) are the unknown magnetic source locations and (x,y,z) are the total field magnetic coordinates. Since a regular grid is used, equation (3) can be solved over a small window. Its size will depend on the magnetic anomaly (or anomalies) extent in the area of study.

The objective is to solve a system of equations over a moving window, as a function of the source anomaly coordinates (Keating, 1998). Good solutions
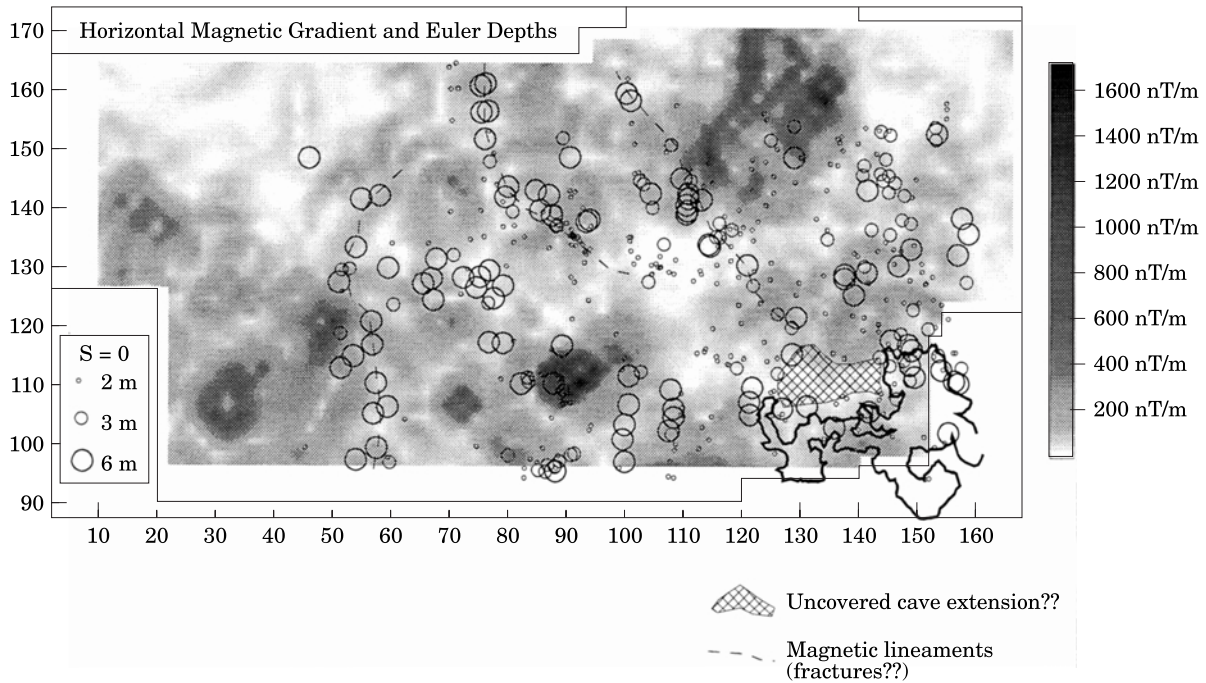
Figure 6. Euler depths superimposed on the horizontal field (Figure 5). Euler depths are shown as circles from 3 to 6 m and computed for a structural index S=0. Observe that boundaries of Las Varillas tunnel are reasonably well delineated by circles, reflecting the depth to the bottom of this structure. Main magnetic lineaments and possible extension for Las Varillas tunnel are also displayed.

are considered to be those that gather well. However, results can be strongly affected by aliasing effects, due to quality of field data and interpolation techniques. Magnetic data in this investigation have been collected in a regular grid to minimize such effects.

Following Keating (1998), expression (4) can be rewritten as:

$$x_0 T_x + y_0 T_y + z_0 T_z + SB = x T_x + y T_y + z T_z + ST,$$

and in matrix form will be:

$$\tilde{A} p = Y. \qquad (5)$$

A solution for (5) in the least squares sense is:

$$p = (\tilde{A}^T \tilde{A})^{-1} \tilde{A}^T Y, \qquad (6)$$

where p is the unknown vector of parameters (source coordinates), $\tilde{A}$ is the field gradients matrix and Y is the vector of known values.

The structural index S in equation 4 plays an important role in the inversion process. Magnetic sources are found by estimating a value of S, which corresponds to a specific magnetic geometry. Reid *et al*. (1990) and Keating (1998) discussed in detail the different values that S may have for different models, like contacts, cylinders, and spheres, among others. They have demonstrated that an inadequate selection of S may lead to divergent solutions, and then Euler depths will not assemble as expected. In the present study, one

structural index is shown (S=0). This is the simpler and more helpful to initially outline a geologic contact. Greater values of S in a complex area like Teotihuacan led to non-convergent solutions. Also, different window sizes were tested. We have finally used an 8 × 8 window with a node interval of 2·5 m.

Figure 6 shows the results for this structural index. Magnetic depths are plotted (as different shaped circles) for an interval of 2 to 6 m. Euler depths have been superimposed on Figure 5 for comparison purposes. Magnetic contacts associated with fractures can be inferred. Low-gradient regions (grey-to-white area) are approximately bordered by the Euler locations, to the west of Las Varillas tunnel. Such a feature could depict a small tunnel (empty or filled) at 3 to 6 m deep (discontinuous line in Figure 6).

Vertical magnetic gradient

A high-resolution vertical magnetic gradient survey was carried out over a smaller portion of the area of study (Figure 7). We used a cesium magnetometer (Geometrics G859). Observations were made between profiles P-395 to the north, and P-295 to the south (shown in Figure 7). This survey was partially located on top of Las Varillas tunnel employing 1 m interval between stations and 1 m between surveyed lines. The purpose of this study was to enhance magnetic signals, which could evidence extensions (tunnels) and geologic features associated with the Las Varillas tunnel or other magnetic sources. Euler transform results were
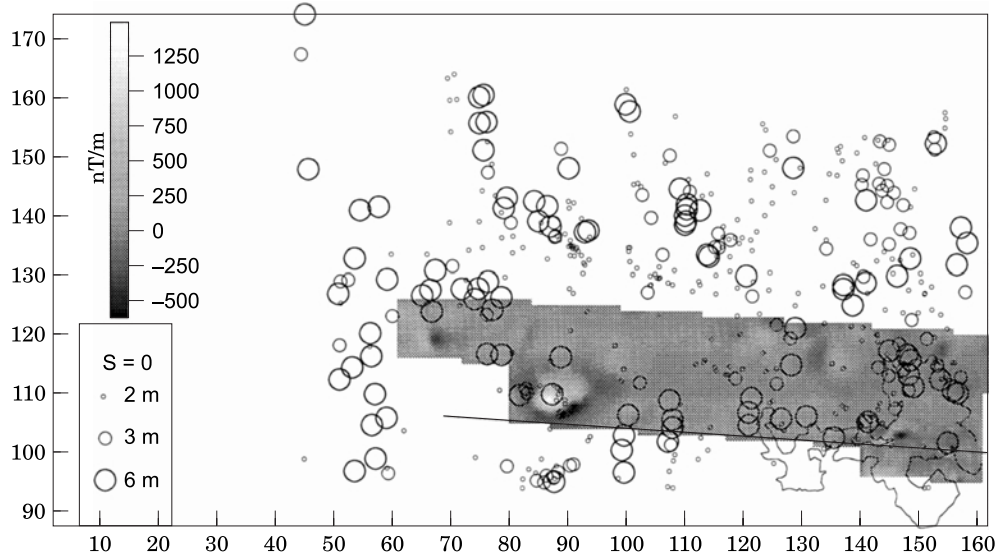
Figure 7. Observed vertical gradient field. A high-resolution survey was carried out on top of Las Varillas tunnel to study it in detail. Euler depths have been also plotted on top. Small dipolar anomalies can be observed in some corners of the cave, delineating basaltic pillars and volcanic bombs.

also plotted on top of the vertical gradient map (Figure 7) for comparison purposes. Magnetic source depths correlate well with the position of the magnetic high, as Barba (1995) reported from the exploration boreholes and the magnetic models proposed by Chávez *et al.* (1994). Other geological features to the left- and right-upper corner are also depicted, probably associated with small basaltic pillars or emission cones, also resolved by the Euler method. Dipolar anomalies can be observed associated with the boundaries of the tunnel, probably representing the basaltic pillars that support the tunnel's roof. Some small high magnetic values are found inside the tunnel's main chamber related to bomb clusters and basalt blocks. Euler depths trace reasonably well the boundaries of the tunnel, whose depth range between 3 m to 6 m (tunnel's top and bottom). It is important to point out that Manzanilla, Lopez & Freter (1996) discovered man and animal burials along archaeological artifacts inside this tunnel.

Ground penetrating radar profiles

GPR represent the new generation of prospecting geophysics systems, which employ electromagnetic waves generation methods. This device is commonly used to define shallow structures based on the reflection of such waves as a function of dielectric properties in the geologic horizons. The electromagnetic waves are sent to the Earth's interior using special designed transmitter antennas and collected after reflection in receiving devices. The dielectric constant ε plays an important role in depth estimation of geological targets. Lateral and vertical variations of it will cause anomalies in the GPR radargrams.

Annan & Davis (1992) established the detectability ranges for these types of systems that depend on the geological targets, and their environment. It is important to point out that penetration of the EM energy will depend on the value of electrical conductivity and ε for each geological layer. In particular, shallow structures (<20 m) may be detected, nevertheless it will depend on the electric conductivity of surficial soil and the number of times the spherical wave hits the same location at depth (stacking). Also, it is important to consider the frequency employed and for bi-static systems the antenna separation. These parameters will help to control vertical penetration of the EM signal and the signal-to-noise ratio.

The GPR EKKO-IV was employed in the present study. This is a bi-static system with two antennas of 100 MHz. Transmitter and receiver were separated 1 m, with observation intervals at 0·5 m. Previously, a velocity analysis was carried out to determine the velocity of the first horizon and the array employed. Therefore an estimate of ε can be obtained. Two profiles were studied P-295 and P-395, which situation is shown in Figures 3 and 5. Profile 295 is displayed in Figure 8(a); the filtered radargram is shown at the bottom. It shows reflections beneath the top of the basaltic flow, at about 2 to 3 m deep. Such features are found at different depths, delineating the cave's roof to the east (discontinuous line), between fiducials 130 and 160. GPR anomalies go slightly deeper towards the west. Multiples are shown in this figure. Observe the behaviour of the magnetic and horizontal gradient fields plotted on top of Figure 8(a). A horizontal gradient high on top of the tunnel's location reveals one of the edges of the structure. The total field shows a conspicuous low to the right end of the plot,

(a)

(b)
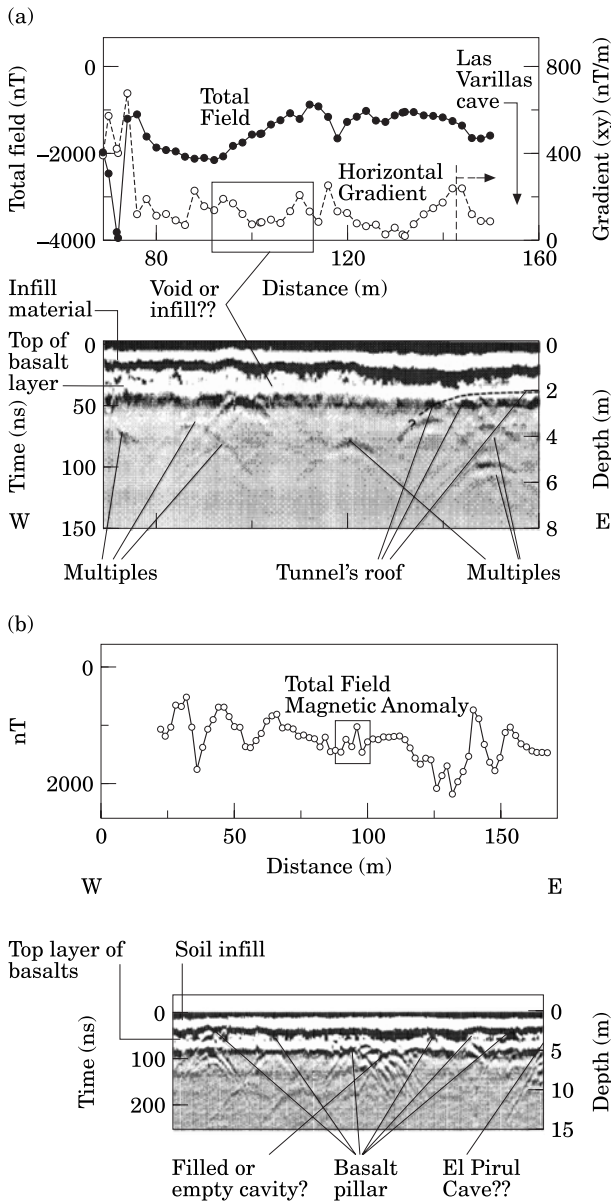
Figure 8. (a) Total magnetic and horizontal gradient profiles are plotted (top) as compared with GPR profile P-295 (bottom). Main geological features are pointed out in this figure. The inferred location of Las Varillas tunnel's roof is outlined with a discontinuous line. (b) Same as (a) for the profile P-395. A more complex geomorphology can be observed in this graph. Magnetic anomalies can be associated to topographic highs in the pyroclastic flow as well as basaltic pillars.

probably related to the tunnel's structure. At point 90, a reflection can be observed at a depth of 3 m, which may be associated with a magnetic anomaly located to the south of Figure 3 (90, 108). Chávez *et al.* (1994) interpreted this feature as a basaltic pillar surrounded by a low-magnetic infill. Note that the horizontal gradient profile possesses two highs with a low in between (square in Figure 8(a)), which defines the extent of the magnetic source. Immediately after, a

structural high within the basalts is defined at fiducial 115.

Figure 8(b) shows the GPR profile P-395. This profile depicts a more complex morphology of the pyroclastic flow. The total field magnetic anomaly has been plotted on top of the radargram for comparison purposes. The magnetic highs could be associated with basaltic pillars or emission cones. At the eastern end an interesting anomalous feature can be observed forming a classical hyperbola (half of it is depicted at the end of the line to the E). It can be associated with El Pirul tunnel, located to a few metres to the northeast of Las Varillas tunnel (Figure 2). A magnetic anomaly located at fiducial 90 (square in Figure 8(b)) correlates with a GPR feature indicating the presence of a basaltic pillar. Immediately after to the W, another signal is located, probably associated with infill material partially filling a small cavity to about 4 m deep. The horizontal magnetic gradient shows very low magnetic values at this position (Figure 5).

Resistivity imaging

Observations are normally made using a computer controlled system with a large number (25 or more) of electrodes laid out in a profile at constant intervals. The data are displayed in a pictorial representation of the variation of resistivity in the subsurface. However, exact depths ascribed to the resistivity values depend upon the subsurface resistivity distribution, and on the electrode geometry.

Electrical imaging can be divided into two steps: (1) data collection process and (2) the inversion approach to estimate the true subsurface resistivity. Mathematical modelling can be done in several steps: (1) apparent resistivity is computed employing a finite difference or finite element method, (2) select the non-linear optimization technique, (3) evaluate the elements of the Jacobean matrix, and (4) solve the system of equations.

Data were collected using a Wenner-Schlumberger array with 3 m electrode spacing and up to 5 levels of determination, which corresponds to a maximum penetration depth of less than 5 m. The method developed by Loke & Barker (1995) was employed to determine the resistivity distribution at depth. The j-observed data is calculated by using a first-order Taylor approximation, as:

$$e_j^{est} = \mathbf{F}_j(\mathbf{P}_{est}) + \sum_{k=1}^{M} \frac{\partial \mathbf{F}_j(\mathbf{P}_{est})}{\partial p_k} \delta p_k \qquad (8)$$

where $j = 1,2,3 \ldots N$. $\mathbf{P}_{est}$ is the estimated parameters vector of the model (resistivities) and if the difference between the observed and computed model response is taken, we obtain:

$$\delta e_j = e_j^{obs} - e_j^{est},$$
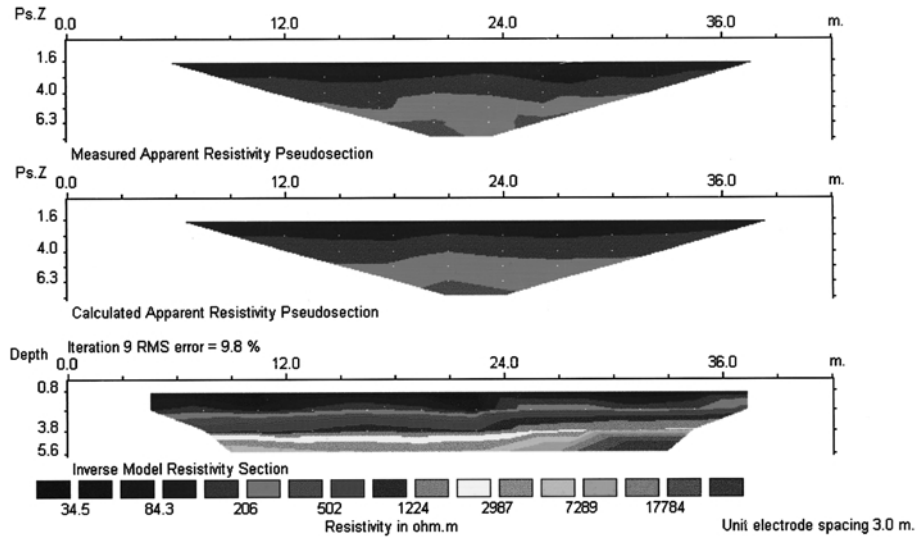
Figure 9. Electric tomography results. Observed apparent resistivity (top) is compared with its computed counterpart (Middle). After nine iterations, the true resistivity distribution is obtained (bottom). Resistivities of cave are larger than 17,700 ohms.m, and its top is at 3·5 m deep. Base could not be defined because profile length was too short.

for each observed data we get:

$$\mathbf{g} = \mathbf{J} \, \delta \, \mathbf{P} \qquad (9)$$

where $\mathbf{J}$ is the Jacobean matrix with elements:

$$J_{j,k} = \frac{\partial F_j}{\partial p_k},$$

and $\delta\mathbf{P}$ is the perturbation vector and $\mathbf{g}$ is the vector of differences. Following Loke & Barker (1995), the equation (9) can be solved for $\delta\mathbf{P}$ as:

$$\delta \, \mathbf{P} = (\mathbf{J}^{\mathbf{T}}\mathbf{J} + \lambda \mathbf{C}^{\mathbf{T}}\mathbf{C})^{-1}\mathbf{J}^{\mathbf{T}}\mathbf{g}. \qquad (10)$$

Here λ is a damping factor and $\mathbf{C}$ is a flatness filter which is used to constrain the smoothness of the perturbations to the model parameters to some constant value (Sasaki, 1992). The upper symbol T indicates the transpose matrix. A method named *least square deconvolution* (Loke & Barker, 1995) is used to estimate the jth element of the Jacobean matrix. The matrix is updated by applying the Broyden's method. Then, it is not necessary to calculate the entire Jacobean matrix for each iteration, the process is more stable and the convergence rate is fast (Broyden, 1972). The mathematical expression for $\mathbf{J}$ can be expressed as (Loke & Barker, 1995):

$$\mathbf{J}_i(\bar{r}) = \frac{\partial U(\bar{r})}{\partial \rho_i} = \frac{I}{4\pi^2} \int_{v_i}$$

$$\frac{x'(x-x')-y'^2-z'^2}{[x'+y'+z']^{3/2}[(x-x')^2+(y-y')^2+(z-z')^2]^{3/2}} \, dV_i.$$

$$(11)$$

The resistivity model consists of a series of contiguous 2-D prisms, where each prism has a constant resistivity. Some authors name this process as Electric Tomography, since the resistivity distribution represents the real earth resistivity. Then, the set of resistivities can be displayed in a grey-tone or a colour scale.

The resistivity profile was taken along profile 295, on top of Las Varillas tunnel (Figure 3). Observed and computed apparent resistivities after nine iterations are shown (Figure 9). The calculated error in the fit is less than 10%. Nevertheless, the resolution obtained in the image is quite good. The final true resistivity section is displayed at the bottom of Figure 9. A high resistivity region is observed to the eastern end of the profile. This defines the uppermost portion of Las Varillas tunnel at a depth of 4 m, approximately. Low resistivity values correspond to the soil infill on top of the layer of basalt. At position 143 (24 in Figure 9), a fault could be inferred cutting the sediments on top of the basaltic horizon located to a depth of 3 m, approximately. This depth agrees well with the mean depth computed by the power spectrum analysis of the magnetic data, as well as with the GPR results. Unfortunately, the length (30 m, approximately) of the resistivity profile did not allowed for a deeper penetration, and its base could not be resolved.

A 2-D general geophysical model

A general model of Las Varillas tunnel can be computed by integrating results from magnetic, GPR and resistivity data. Figure 10 displays such an integral model. A vertical magnetic gradient field profile interpolated from data of Figure 7 was interpreted (Figure 10(a)). We have employed a 2-D gravity-magnetic
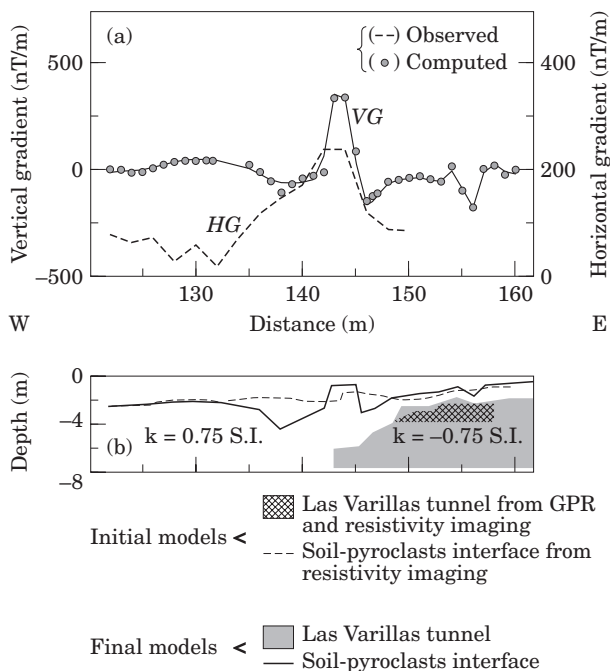
Figure 10. Integral geophysical interpretation on top of Las Varillas tunnel. A vertical gradient profile obtained from Figure 7(a) along profile P-295 has been inverted. The horizontal magnetic gradient (HG) is also displayed for comparison purposes (a). Position of the soil-pyroclastic flow interface (discontinuous line, b) and cave inferred from the electric tomography and GPR results were used as initial models to constrain magnetic inversion (b) (Interpex, 1998).

modelling package (INTERPEX@, 1998) to model the data. The vertical magnetic gradient field could be inverted, constraining the inversion process with the GPR and resistivity results (Figure 10(b), initial models for the tunnel and infill material-pyroclast flow interface are shown, see also Figures 8(a) & 9). A final solution was computed after five iterations and the error in the fit was decreased to less than 1%. The magnetic model of Las Varillas tunnel reproduces the entire view of the structure. Its bottom is inferred at a depth of 8 m, approximately, and extends in the E–W direction for almost 20 m from its main entrance. A structural prominence of the pyroclastic sheet may be responsible of the anomalous high observed in the vertical magnetic gradient profile. The resistivity image of the tunnel was used to infer the initial model employed (shown in Figure 10). It is important to point out that the resistivity and GPR results were used to constrain the final magnetic model computed.

Conclusions

A multicomponent geophysical study has been carried out to determine the possible existence of tunnels to the east of the Pyramid of the Sun at the ancient archaeological city of Teotihuacan. Combined mathematical approaches applied to the magnetic data helped to characterize the geology of the subsurface. A possible

extension of Las Varillas tunnel was inferred from the Euler and horizontal magnetic gradient maps. Also, important information was provided to infer the location of magnetic features employing the observed vertical magnetic gradient.

GPR radargrams showed the location at depth of the uppermost section of the Las Varillas tunnel. The correlation between GPR results and the magnetic gradients defined the position of basaltic pillars and emission centres as well as possible cavities or infill zones. The GPR profiles clearly showed the sedimentary cover above the pyroclast sheet, with an average thick of 3 m.

Resistivity imaging carried out along GPR profile P-295 constrained the inversion of the vertical gradient data. An integral model of Las Varillas tunnel was obtained. An extension of this feature could be estimated that might be of archaeological interest. Structural alignments inferred may be associated with fractured zones in the pyroclastic flow. Infill zones were estimated within the area of study.

References

Annan, A. P. & Davis, J. L. (1992). Design and development of a digital ground penetrating radar. In (J. A. Pilon, Ed.) *Ground Penetrating Radar*. Geological Survey of Canada **90–4**, pp. 15–23.

Arzate, J. A., Flores, L. E., Chávez, R. E., Barba, L. A. & Manzanilla, L. (1990). Magnetic Prospecting for tunnels and caves in Teotihuacan, Mexico. In (S. H. Ward, Ed.) *Geotechnical and Environmental Geophysics: Investigations in Geophysics* **5**. Society of Exploration geophysicists, **III**, pp. 155–162.

Barba, L. A., Manzanilla, L., Chávez, R. E., Flores, L. E. & Arzate, J. A. (1990). Caves an tunnels at Teotihuacan, Mexico: A geological phenomenom of archaeological interest. In (N. P. Lasca & J. Donahue, Eds) *Archaeological Geology of North America: Boulder, Colorado*. Geological Society of America, Centennial Special **4**, pp. 431–438.

Barba, L. A. (1995). *Impacto humano en la paleogeografía de Teotihuacan*. Ph.D. Thesis, Facultad de Filosofía y Letras. UNAM, México.

Basante, O. R. (1982). Algunas cuevas en Teotihuacan. In (R. Cabrera-Castro, I. Rodriguez & N. Morelos, Eds) *Memoria del Proyecto Arqueológico Teotihuacan 80–82*. Colección Científica, Arqueología (INAH-México), **132**, pp. 341–354.

Broyden, C. G. (1972). Quasi-Newton methods. In (W. Murray, Ed.) *Numerical Methods for Unconstrained Optimization*. Academic Press, pp. 87–106.

Campos-Enriquez, O., Flores-Marquez, E. L. & Chávez, R. E. (1997). Geophysical characterization of hydrogeologic systems. *The Leading Edge* **12**, 1769–1773.

Chávez, R. E., Manzanilla, L., Peralta, N., Tejero, A., Cifuentes, G. & Barba, L. A. (1994). Estudio Magnético y de resistividad en los alrededores de la pirámide del Sol, Teotihuacan, México. *Geofísica Internacional,* **33**, 243–255.

Chávez, R. E., Hernández, M. C., Herrera, J. & Cámara, M. E. (1995). A magnetic survey over La Maja, an archaeological site in Northern Spain. *Archaeometry,* **37**, 171–184.

Chávez, R. E., Tejero, A. & Urbieta, J. (1998). Cavity detection in urban zones of Mexico City: *Proceedings of the IV Meeting of the EEGS* (European Section), 355–358.

Heyden, D. (1975). An interpretation of a cave underneath the Pyramid of the Sun in Teotihuacan, Mexico: *American Antiquity* **40**, 131–147.

Heyden, D. (1981). Caves, gods and myths: worldviews and planning in Teotihuacan. In (E. P. Beson, Ed.) *Mesoamerican Sites and Worldviews*. Dumbarton Oaks Research Library and Collection, pp. 1–39.

Hildebrand, A. R., Pilkington, M., Connors, M., Ortiz-Aleman, C. & Chávez, R. E. (1995). Size and structure of the Chicxulub crater revealed by horizontal gravity gradients and cenotes. *Nature* **376**, 415–417.

INTERPEX (1998). MAGIXP[plus], *magnetic and gravity interpretation software users manual*.

Keating, P. B. (1998). Weighted Euler deconvolution of gravity data. *Geophysics* **63**, 1595–1603.

Loke, M. H. & Barker, R. D. (1995). Least squares deconvolution of apparent resistivity pseudosections. *Geophysics* **60**, 1682–1690.

Manzanilla, L., Barba, L. A., Chávez, R. E., Tejero, A., Cifuentes, G. & Peralta, N. (1994). Caves and Geophysics: an approximation to the underworld of Teotihuacan, México. *Archaeometry* **36**, 141–157.

Manzanilla, L., López, C. & Freter, A. (1996). Dating results from excavations in quarry tunnels behind the pyramid of the Sun at Teotihuacan. *Ancient Mesoamerica* **7**, 245–266.

Milán, M. (1990). Estudio geológico-geofísico para la detección de cavernas en la zona arqueológica de Teotihuacan, Edo. de México. *Internal Report IIA-UNAM*, México, 200 pp.

Mooser, F. (1968). Geologiá, naturaleza y desarrollo del Valle de teotihuacan: in: Materiales para la Arqueología Teotihuacana. In (J. L. Lorenzo, Ed.) *Internal Publication INAH-México,* **17**, pp. 29–37.

Reid, A. B., Allsop, J. M., Granser, H., Millet, A. J. & Somerton, I. W. (1990). Magnetic interpretation in three dimensions using Euler deconvolution. *Geophysics* **35**, 180–191.

Sasaki, Y. (1992). Resolution of resistivity tomography inferred from numerical simulation. *Geophysical Prospecting* **40**, 453–464.

Spector, A. & Grant, F. S. (1970). Statistical models for interpreting aeromagnetic data. *Geophysics* **35**, 293–302.

Soruco, E. (1985). *Una cueva ceremonial en Teotihuacan.* Unpublished M.A. Thesis, Escuela Nacional de Antropología e Historia, Mexico.